Solute nanostructures and their strengthening effects in Al-7Si-0.6Mg alloy F357

G. Sha[a,#], H. Möller[b,*], W.E. Stumpf[c], J.H. Xia[a], G. Govender[b], S.P. Ringer[a]

[a] *Australian Centre for Microscopy & Microanalysis, The University of Sydney, Madsen Building F09, NSW 2006, Australia.*

[b] *Council for Scientific and Industrial Research, Materials Science and Manufacturing, PO Box 395, Pretoria, South Africa, 0001.*

[c] *Department of Materials Science and Metallurgical Engineering, University of Pretoria, Pretoria, South Africa, 0001.*

Corresponding author: gang.sha@sydney.edu.au; Tel: +61 29 036 9050; Fax: +61 29 351 7682.

* Corresponding author: hmoller@csir.co.za; Tel: +27 12 841 2139; Fax: +27 12 841 3378.

Abstract

The solute-nanostructures formed in the primary α-Al grains of a Semi-Solid Metal cast Al-7Si-0.6Mg alloy (F357) during ageing at 180°C, and the age-hardening response of the alloy have been systematically investigated using transmission electron microscopy, atom probe tomography and hardness testing. A 120-h natural pre-ageing led to the formation of solute clusters and GP zones. The natural pre-ageing slowed down the precipitation kinetics six-fold during 1 h ageing at 180°C, but this effect diminished after 4 h when the sample reached the same hardness as that without the pre-ageing treatment. It reduced the number density of β″-needles to approximately half of that formed in samples without the treatment, and postponed the peak hardness occurrence to 4 h, 4 times that of the as-quenched sample. A hardness plateau developed in the as-quenched sample between 1 h and 4 h ageing corresponds to the growth of

the β″ precipitates and a significant concurrent decrease of solute clusters and GP zones. The average Mg:Si ratio of early solute clusters is < 0.7 while that of GP zones changes from 0.8 to 0.9 with increasing in their size, and that of β″-needles increases from 0.9 to 1.2. β″-needles, GP zones and solute clusters are important strengthening solute nanostructures of the alloy. The partitioning of solutes and precipitation kinetics of the alloy are discussed in detail.

Keywords: Solute nanostructure; Precipitation; Cast aluminium alloys; Atom probe tomography; TEM.

1. Introduction

Casting alloys Al-7Si-Mg A356/7 are used for critical castings in aircraft such as the engine support pylons and automotive components such as wheels and cylinder heads [1,2]. They contain 6.5 - 7.5% Si, which is significantly higher than that of the 6000 series Al alloys of generally ≤ 1.5% Si [3]. The typical microstructures of these alloys consist of primary α-Al grains and eutectic structures. In the as-cast condition, the primary α-Al grains are much softer than the eutectic structures. Ageing treatment is required to strengthen the primary α-Al grains in order to enhance the overall strength of the alloys.

Precipitation in the α-Al grains of the cast Al-Si-Mg alloys has seldom been investigated in detail. In contrast, the precipitation of the 6000 series alloys has been studied extensively and the decomposition of the supersaturated solid solution (SSSS) is believed to occur in a sequence as follows [4-6]:

$$SSSS \rightarrow (Mg + Si)_{clusters} / GP\text{-}I_{spherical} \rightarrow \beta'' / GP\text{-}II_{needles} \rightarrow \beta_{rods}' \rightarrow \beta \quad (+ Si)$$

where GP denotes Guinier-Preston zones, β′ and β″ are metastable precursors of β (with β′ = $Mg_{1.7}Si$ and β″ = Mg_5Si_6 and β = equilibrium Mg_2Si) [4,5]. It is usually assumed that β″ consists of only Mg and Si, but significant quantities of Al have been detected in these precipitates [6,7]. Solute clusters are important for the evolution of the precipitation microstructure. However, the precise nature of solute clusters in Al-Mg-Si wrought Al alloys is far from clear yet, and remains an important topic attracting significant research interests [6,8-11]. Previous research using 1D atom probe (1DAP) suggested three types of solute clusters i.e. Mg clusters, Si clusters and Mg-Si clusters, based on a few solute-rich features detected. Since a 1DAP analysis was typically from a region of 1-2 nm in diameter and suffered from the lack of lateral resolution, the analysis was unable to distinguish between partial and whole clusters detected. The uncertainty makes the

1DAP analysis not suitable to detect the precise chemistry of each single cluster given that those earlier solute clusters likely have a range of compositions. Failing to address the limitations of the 1DAP analysis makes some previous interpretations about the chemical characteristic of small solute clusters problematic. This may explain why pure Mg and Si clusters were not observed in later 3DAP measurements [6,11] and there are conflictions among different 1DAP results [8-10].

The influence of prior natural ageing time on the subsequent artificial ageing response of Al-Mg-Si wrought alloys has been an interesting topic and has attracted a lot of research interest [3,12-16]. In the 6000 series alloys with high alloying element concentrations, clusters formed during natural ageing have been considered to be "robust" during subsequent artificial ageing [1,12]. They are believed to trap the available vacancies, but they do not serve as favourable sites for heterogeneous nucleation of β″ [16]. For instance, in alloy 6082 artificially aged immediately after a solution treatment, the number density of β″ precipitates has been reported to be almost five times higher than that of samples naturally aged for a week followed by the same artificial ageing [12]. This has an adverse effect on the tensile properties of the alloy [1,15]. The opposite, however, is believed to occur in the 6000 series alloys with low alloying element addition [1,13,15]. Chang and co-workers [13] described a "positive effect" of natural pre-ageing on precipitation hardening in an Al-0.44at%Mg-0.38at%Si alloy, i.e. natural pre-ageing led to an increase in peak hardness compared to samples without prior natural ageing. In this case, some of the clusters formed during natural ageing are postulated to act as nucleation sites for β″, resulting in smaller needles at a higher number density [13].

In Al-7Si-Mg casting alloys, natural pre-ageing causes a sluggish age-hardening response during subsequent artificial ageing, but interestingly, the extent of the loss in hardness is fully recovered

upon further artificial ageing [17-19]. To date, there is a lack of detailed research revealing precipitate micro- and nanostructural evolution during ageing of Al-Si-Mg casting alloys. The influence of natural ageing on subsequent artificial ageing of Al-Si-Mg-(Cu) casting alloys is not yet fully understood [20]. It is believed that a better understanding of the precipitation behaviour of Al-7Si-Mg casting alloys could lead to optimized heat treatments to improve the alloy's performance and could benefit in new alloy design [2]. The objective of this research is to evaluate the formation of solute-nanostructures in the α-Al grains using advanced atom probe tomography (APT) and transmission electron microscopy (TEM) and to unveil the characteristics of solute clusters, GP zones and β″ formed in the alloy under different ageing conditions. This research aims to develop a deeper understanding of the nanostructural evolution of Al-7Si-Mg alloys and to reveal the effects of natural pre-ageing on precipitation kinetics during subsequent artificial ageing in this alloy.

2. Experimental Methods

Al-7Si-0.6Mg alloy F357, with chemical compositions listed in Table 1, was prepared from semi-solid metal (SSM) slurries using the Council for Scientific and Industrial Research Rheocasting System (CSIR-RCS) [21], Macro-Vickers hardness (VHN) measurements were performed using a 10 kg load with a standard deviation of ± 3 VHN. Micro-Vickers hardness measurements on the primary α-Al and the eutectic components were performed using a 50 g load. A solution treatment was conducted at 540°C for 1 h, and then the samples were quenched in water. Further artificial ageing was conducted at 180°C for up to 4 h. A T4 treatment was performed at room temperature for 120 h. The tensile tests were performed using an INSTRON 1342/H1314, with 4 samples tested for each data point.

Thin foils for transmission electron microscopy (TEM) were prepared from 3 mm discs by using twin-jet electro-polishing in a solution of 30% nitric acid in methanol at -30°C. TEM examinations were performed using a Philips CM120 TEM operated at 120 kV. Tip samples for APT analysis were prepared from blanks with dimensions of $0.3\times0.3\times15mm^3$ using a two-stage electropolishing technique [22]. The first stage used a solution of 25% perchloric acid in acetic acid at 15V, whereas the second stage used an electrolyte of 5% perchloric acid in 2-butoxyethanol at 20V. APT analysis was done under an ultrahigh vacuum (~ 1×10^{-8} Pa) at ~ 20 K, and a voltage pulse fraction of 20%, using a Local Electrode Atom Probe (LEAP3000X SI®) and having at least 20 million atoms collected for each data set. Imago Visualization and Analysis Software (IVAS^{TM}) in combination with advanced calibration techniques was used in APT data reconstruction and visualization [23,24]. The maximum separation algorithm was employed for cluster identification [7], with Mg, Si and Cu as clustering solutes, a separation distance of 0.6 nm, a surrounding distance of 0.5 nm to include all other elements, and the minimum cluster size of n = 10 to reduce the effect of small solute clusters that exist in the alloy with solutes in a random distribution [25-27].

3. Results

3.1. Age hardening response and tensile properties of SSM-HPDC F357 alloy

Hardness curves of SSM-HPDC processed F357 alloy samples during ageing at 180°C with or without a natural pre-ageing (T4 treatment) are shown in Figure 1. A hardness plateau of 120 VHN was found between 1 and 4 hours for the samples without the natural pre-ageing. In contrast, no such a plateau, but the peak hardness of 120 VHN at 4 h was observed for the samples experienced the T4 treatment. The hardness of the primary α-Al is very close to the

macrohardness of the alloy, but the hardness of the eutectic structure is higher. This demonstrates the importance of strengthening primary α-Al grains of the cast alloy, as observed in alloy A356 [28].

Table 2 shows tensile properties of the samples aged for different conditions. The tensile test results correlate well with the hardness curves shown in Fig. 1. The as-quenched samples artificially aged for 1 h and 4 h had the same hardness (Fig. 1), similar ultimate tensile strengths (UTS), but different yield strengths (YS) and ductilities (Table 2). The 1 h sample had a significantly lower YS and slightly higher ductility than the 4 h sample. The samples artificially aged for 4 h with or without the natural pre-ageing are similar in YS, UTS and ductility.

3.2. TEM observations of solute nanostructures in the SSM-HPDC F357 alloy

Figure 2 shows $<001>_{Al}$ bright field (BF) TEM images and corresponding selected area diffraction patterns (SADPs) of T4-treated F357 alloy samples aged at 180°C for up to 4 h. Except for dislocations, no precipitates are observed in the BF images of the T4 sample and the 180°C-10min sample in Fig. 2a and 2b respectively. This is consistent with only diffraction spots of the Al matrix observed in SADPs. After ageing at 180°C for 1 or 4 h, streaks were clearly observed in the $<001>_{Al}$ SADPs of the samples as shown in Figs. 2c and 2d. This corresponds to the needle-like β″ precipitates in dark contrast in the BF images (Figs. 2c and 2d) [29]. With the increase in ageing time from 1 h to 4 h at 180°C, the sizes of β″-needles increased from ~ 2 nm diameter × 10 nm length to ~ 4 nm diameter × 25 nm length in the pre-aged samples (Figs. 2c and 2d).

Figure 3 shows BF images and SADPs of the samples that experienced no natural pre-ageing prior to artificial ageing at 180°C for up to 4 h. Faint streaks in the $<001>_{Al}$ SADP of the sample

aged for 10 minutes at 180°C, as shown in Fig. 3a, indicated the limited precipitation of β″ in dark contrast (~ 2 nm diameter) in the BF image. After ageing for 1 and 4 h at 180°C, the intensity of streaks in the SADPs (Figs. 3b and 3c) increased significantly, indicated that more β″- needles formed [8]. With the increase in ageing time from 1 h to 4 h at 180°C, the sizes of β″-needles in the samples without the pre-ageing treatment increased from ~ 3 nm diameter × 20 nm length to ~ 4 nm diameter × 25 nm length (Figs. 3b and 3c).

3.3 APT examination of the solute nanostructures of the F357 alloy

Figure 4 shows three-dimensional (3D) reconstructed Mg atom maps containing only solute-enriched features in the samples experienced 120 h natural ageing before artificial ageing at 180°C for up to 4 h. Only equiaxed solute-rich features, i.e. clusters and GP zones, were observed in the sample in the T4 condition and that aged at 180°C for 10 min as shown in Figs. 4a and 4b respectively. After ageing for 1 h, only a few β″-needles were evidenced with the remainder equiaxed solute-rich features (Fig. 4c). After ageing for 4 h (peak-aged sample), β″ precipitates are dominant as shown in Fig. 4d. It is difficult to make a scientific distinction between GP zones and solute clusters because of their similar spherical morphologies [4]. Critical sizes of 8 and 30 solutes have previously been used to distinguish between solute clusters and GP zones in wrought Al-Mg-Si alloys [6,30]. In this research, all solute-rich features were divided into three groups according to their sizes. Considering a detection efficiency of ~55% in APT analysis, a spherical feature of 1 nm in diameter should be detected containing about 30 atoms. We used 20 solutes as a critical size assuming that 1/3 detected atoms will be Al atoms. The small solute-rich features containing 10-20 detected solute atoms are designated as solute clusters. Those containing 21-100 solute atoms are GP zones, and elongated β″ contains > 100 solute atoms.

Figure 5 shows Mg atom maps containing only solute-enriched features after removing solutes in the matrix of samples experienced no natural ageing prior to artificial ageing at 180°C for up to 4 h. Ageing for 10 min at 180°C caused the formation of larger equiaxed solute-rich features in a high number density, as shown in Fig. 5a. After ageing for 1 h, significant amounts of β″-needles, (Fig. 5b) formed in the alloy. After ageing for 4 h, β″-precipitates are dominant in the microstructure.

3.3.1. Number density evolution of precipitates

Figure 6 shows the evolution of the number density of solute-rich features in alloy F357 samples with/without natural pre-ageing during ageing at 180°C for up to 4 h. The T4 sample contains only high number densities of solute clusters (2.28×10^{24} m^{-3}) and GP zones (5.41×10^{23} m^{-3})(Fig. 6a). Further ageing of the T4 sample at 180°C for 10 min leads to a slight decrease in the number density of solute clusters (2.21×10^{24} m^{-3}), but a slight increase in the number density of GP zones (6.68×10^{23} m^{-3}). Further ageing for 1 h leads to the transformation of clusters into GP zones, with a decrease of the cluster number density (1.53×10^{24} m^{-3}) but an increase in GP-zone number density (9.52×10^{23} m^{-3}), as well as the formation of small β″-needles at 1.15×10^{23} m^{-3}. Ageing for 4 h at 180°C results in a significant decrease in solute clusters (4.31×10^{23} m^{-3}) and GP zones (1.57×10^{23} m^{-3}), but an increase in β″-needles number density (1.49×10^{23} m^{-3}) and size, which provide the peak hardness (Fig. 1) and strength (Table 2).

The evolution of the number density of solute-rich features in the alloy without the T4 treatment is largely different from that experienced the T4 treatment during ageing at 180°C. The as-quenched sample aged for 10 min at 180°C produced not only solute clusters and GP zones, but

also small β″-needles containing 101-400 solute atoms in a number density of 7.60×10^{22} m^{-3} (Fig. 6b). This is in good agreement with the faint streaks observed in the <001> SADP of the sample (Fig. 3a). Further artificial aging to 1 h caused a significant increase in the number density and size of β″-needles (3.29×10^{23} m^{-3}), but a decrease in the number density of both solute clusters and GP zones. After ageing for 4 h, the number density of large β″-needles with more than 1200 solute atoms increased almost 8 times to 1.88×10^{22} m^{-3} (Fig. 6b), but the number density of solute clusters decreases almost 12 times and that of GP zones decreases to 8.45×10^{22} m^{-3}. This coincides with the hardness plateau as shown in Fig. 1.

3.3.2. The evolution of chemistry of clusters and precipitates in alloy F357

The Mg:Si ratios of solute clusters, GP zones and β″-needles in samples with or without the T4 treatment prior ageing at 180°C are shown in Figure 7. The Mg:Si ratio of the solute-rich features increases with artificial ageing time as the decomposition of the supersaturated solid solution proceeds from clusters to GP zones to β″. The early solute clusters formed after 10 min ageing are Si-rich with a Mg:Si ratio of 0.7, less than 0.83, the theoretical ratio of β″[1,4]. A similar Mg:Si ratio was reported for solute clusters in an Al-7Si-0.3Mg alloy A356 [2]. The needles with > 1200 solute atoms have a Mg:Si ratio of ~ 1.0 – 1.2 (less than 1.7 for β′), which is in agreement with the ratio of 1.2 found for β″-needles in the peak aged Al-7Si-0.3Mg alloy A356 [2].

Significant quantities of Al have been detected in all precipitates in this study. On average, the solute clusters were found to contain ~ 3.7 at% Mg and 5.5 at% Si, the GP zones ~ 6.1 at% Mg and 6.5 at% Si and the β″-needles ~ 10.5 at% Mg, and 9.3 at% Si. Similar results have also been reported in wrought alloy 6061-T6 [6] and an Al–Mg–Si–Cu alloy containing an excess of Si [7].

Structural models that accommodate Al atoms in β″-needles and GP zones have been proposed based on TEM studies [31,32]. The F357 alloy contains Cu at 0.02 at% (Table 1). Small solute clusters were detected having weak Cu-enrichment, as shown in Fig. 8. With increasing in ageing time, the Cu concentration of the GP zones increased. β″ precipitates were observed with higher Cu enrichment than both the GP zones and solute clusters.

3.3.3. The matrix composition evolution

The solute-concentration evolution in the matrix of F357 alloy samples with/without the T4 treatment during ageing at 180°C for up to 4 h is illustrated in Figure 9. The Mg and Si contents of the analysed volume (a primary α-Al grain) in the T4 condition are 0.51 and 1.48 at% respectively. The Si content is in reasonable agreement with ~ 1.3 wt% Si detected in the matrix of an Al-7Si-0.5Mg alloy by electron probe microanalysis (EPMA) [33]. Ageing at 180°C for 10 min of the T4 sample did not result in a significant change in the composition of the matrix. However, further artificial ageing causes a gradual decrease in the matrix solute content due to precipitation. The Mg concentration in the matrix decreased from 0.35 at% to 0.12 at%, and the Si concentration in the matrix decreased from 1.41 at% to 1.04 at% during ageing from 1 h to 4 h at 180°C. For the alloy without the T4 treatment, a short 10 min ageing at 180°C resulted in a large decrease in the matrix solute concentrations to 0.43 at% Mg and 1.40 at% Si measured in the matrix. This is consistent with more GP zones and β″ precipitates formed in the alloy as shown in Fig. 6. Further ageing from 1 h to 4 h caused a decrease in the Mg concentration of the matrix from 0.25 at% to 0.11 at% Mg and a decrease of the Si concentration of the matrix from 1.23 at% to 1.13 at% Si.

4. Discussion

TEM and APT examinations confirmed the coexistence of solute clusters, GP zones and β″ in the primary α-Al grains of the casting Al alloy after ageing at 180°C for 4 h. No significant Si clusters and Si-precipitates were observed. This is consistent with previous work reporting the observation of Si precipitates only in over-aged microstructure of a similar casting alloy A356/7 aged at 180°C for 196h [2]. This also appears to be consistent with previous results of wrought Al-Mg-Si alloys with excess Si, i.e. no Si precipitates were observed during early-stage precipitation without the formation of equilibrium β (Mg_2Si) [8,11,12,32,36]. Therefore, the precipitation sequence of the alloy during ageing for up to 4 h at 180°C (the peak aged condition) can be summarised as follows:

SSSS → solute clusters → solute clusters + GP-zones → solute clusters + GP-zones + $\beta''_{needles}$

A natural pre-ageing treatment did not alter the precipitation sequence, but it did affect precipitation kinetics and the relative proportion of solute clusters, GP zones and β″-needles formed in the microstructure of the alloy (details of which will be discussed in the following sections).

4.1. The partitioning of solutes during precipitation of the Alloy F357

Quantitative APT measurement confirmed that early solute-clusters were richer in Si with average Mg:Si ratios in the range of 0.6-0.7, as shown in Fig. 7. This ratio is significantly higher than the Mg:Si ratio (0.29) of the primary α-Al grains. The average Mg:Si ratio of solute clusters in the T4 condition was 0.6, less than 0.7 in the sample shortly aged for 10 min at 180°C. The low Mg:Si ratio of the solute clusters formed at room temperature appears to be consistent with

the strong Si-Si pair correlation as suggested for AA6016 after a long storage at room temperature [10]. In addition, Mg-Si correlation must be significant, otherwise, the Mg:Si ratio of solute clusters will not reach 0.6 > 0.29 of the α-Al grains. Interestingly, after a short ageing for 10 min at 180°C, solute clusters formed from the samples with or without T4 treatment have the same average Mg:Si ratio of ~ 0.7 and similar number density of ~ 2.2×10^{24} m^{-3}. Assuming that short-range ordering is correlated with cluster chemistry, the same cluster chemistry probably suggests that the formation of new short-range-ordering from a pre-existing short-range ordering is very quick at 180°C. The chemistry of pre-existing small clusters may not be a dominant factor to influence the precipitation kinetics of the alloy at 180°C. This conclusion is further supported by the same chemistry of small GP zones containing 21-50 solutes observed from the T4 sample and the as-quenched sample aged for 10 min at 180°C, as shown in Fig.7. The strong interactions of Si-Si and Si-Mg and the fast diffusion of Si likely facilitated forming clusters with a low average Mg:Si ratio. Indeed, the diffusivity of Si in Al at 180°C is estimated to be 3.8×10^{-19} m^2/s, twice that of Mg in Al (1.9×10^{-19} m^2/s), using Arrhenius parameters given by Du et al [34].

After 10 min ageing at 180°C, the T4 sample slightly increased the total number density of solute nanostructures from 2.82×10^{24} (T4) to 2.88×10^{24} m^{-3}, less than 3.61×10^{24} m^{-3} in the sample without natural pre-ageing prior ageing for the same time. Further ageing to 1 h at 180°C, the solute-clusters quantity of the T4 samples decreased 33% (to 1.53×10^{24} m^{-3}), which is lower than the 62% decrement (to 8.32×10^{23} m^{-3}) observed from the samples without the T4 treatment. It is noteworthy that the average Mg:Si ratio of these residual solute clusters remained at 0.6 in the thermally aged T4 sample. This probably implies that solute clusters with low Mg:Si

ratios formed during natural pre-ageing are difficult to transform during subsequent ageing at 180°C, as suggested previously by Yamada et al [16].

The formation of GP zones from solute clusters involved the further enrichment of Mg and increases in their sizes and average Mg:Si ratios in the range of 0.7-0.9. Larger GP zones exhibit higher Mg:Si ratios. It has been suggested that the Mg:Si ratio of most well-developed GP zones is 0.833 in a 6082 Al alloy (with a Mg:Si ratio of 1.8) [32]. This value is in reasonable agreement with the average values of larger GP zones observed in the primary α-Al grains of the cast Al-Si-Mg alloy (with a Mg:Si ratio of 0.29), but is higher than the value of small GP zones which likely just transformed from solute clusters. This indicated that alloy Mg/Si ratio has no significant influence on the chemistry of GP zones, and the growth of GP zones involves further enhanced enrichment of Mg.

β″-precipitates were observed with an Mg:Si ratio in the range of 0.9-1.2, and larger β″ precipitates exhibited a ratio close to 1.2. Previous atom probe measurements produced great inconsistency in the chemistry of β″ precipitates [8,9]. This is largely due to the poor statistics of only few precipitates detected in previous atom probe measurements. Recent first-principle calculations suggest that the lowest formation enthalpy configuration of β″ has a Mg:Si ratio of 1.25 [35], which is consistent with 1.2 detected among the large β″ precipitates in the alloy. Since the β″ precipitates are transformed from large GP zones, it is reasonable to believe that β″ precipitates should have a range of compositions as demonstrated by this research. The formation of β″-precipitates from GP zones was likely controlled by the diffusion of Mg, since Mg diffusivity is lower than that of Si at 180°C. This observation appears to be consistent with previous suggestion that Si atoms control and enhance nucleation of solute clusters, whereas

subsequent growth into GP zones and the formation of β″-precipitates are controlled by the slower diffusing Mg [3,4,13].

It is worth noting that between 10 min and 4 h of ageing at 180°C, the precipitation is in the growth regime as indicated by the decrease in the matrix Mg and Si concentrations (Figs. 9 and 10). Most of the Si and Mg from the matrix assisted the growth of β″ precipitates. A small fraction of Si might goes to solute clusters and small GP zones to lower their Mg/Si ratio in the naturally pre-aged samples (Fig. 7). In the growth regime, although the relative amount of Si (to Mg) in the large β″ precipitates decreases, the growth of the precipitates consumes Si from the matrix. This is consistent with the absence of pure Si precipitates observed at this stage. In coarsening regime, the further increase in Mg/Si ratio of precipitates could cause the precipitation of Si. This is probably the case as previously reported for Al-Mg-Si alloys with excess Si in an over-aged condition [2,12,32,36].

4.2. Formation of solute nanostructures during artificial ageing of F357 samples

The number density of solute clusters (2.28×10^{24} m^{-3}) in the T4 sample is more than 4 times that of GP zones (5.41×10^{23} m^{-3}), as shown in Fig. 6a. The slight decrease in the number density of solute clusters is concurrent with a slight increase in the number density of GP zones during ageing for 10 minutes at 180°C. The dissolution of room-temperature clusters during artificial ageing has been inferred from differential scanning calorimetry (DSC) before [36]. If this process occurred in the F357 alloy with any significance, the dissolution of clusters should result in an increase in Mg and Si concentrations of the matrix after ageing for 10 min at 180°C. The fact that no such increase in Mg and Si concentrations of the matrix were observed, as

shown in Fig. 9, indicates that the dissolution of solute clusters is probably not significant. The coalescence of some small solute clusters most likely occurred in the alloy, as has been postulated for Al alloy 7050 [37].

Precipitation of GP zones and β″ precipitates during further ageing for 1 h and 4 h results in a decrease in the Si and Mg contents of the matrix (Fig. 9). The precise formation mechanism of β″ remains unclear due to the lack of detailed experimental evidence, although it has been assumed that the formation of β″-needles is by heterogeneous nucleation from GP zones [8,12]. The chemistry vs. size profiles of GP zones and β″ obtained by the APT analysis, as shown in Figs. 6-9, clearly demonstrate the continuous evolution between the two. It is therefore reasonable to believe that the formation of β″ is by the transformation of the large GP zones, because their chemistry and size are much closer to those of the small β″ precipitates. The co-existence of GP zones and β″ over longer thermal ageing periods indicates that not all of the GP zones transform into β″. It is probably only those GP zones with size and composition close to β″ that have a strong tendency to transform into β″. The increases in both the number density and size of β″-needles after ageing for 4 h eventually provide the peak hardness (Fig. 1) and peak strength (Table 2) of the alloy.

4.3. Precipitation kinetics and hardening effects during artificial ageing of alloy F357

The reduction in relative solute-concentration of the matrix can reflect the progress of the precipitation process. Fig.10 shows the relative solute-concentration reductions measured from the matrix of naturally pre-aged (T4) and as-quenched samples during ageing at 180°C. This parameter measured from the matrix of the T4 sample aged for 1 h is close to that of the as-quenched sample aged for 10 min. This indicates that the prior natural ageing has slowed down

the precipitation six-fold in comparison with the as-quenched sample during ageing at 180°C, which is most likely due to a decrease in vacancy concentration after the natural ageing. Interestingly, after ageing for 4 h at 180°C, the relative reductions of the matrix solute concentrations detected in the two samples reached the same level. This indicates that the decomposition of the supersaturated solid solution in the two respective microstructures has developed to a similar stage. The initial vacancy concentration difference between the two samples has little influence on the long-term precipitation process after 4 hour ageing. After 1 h ageing at 180°C, the vacancy concentrations of the two samples appear to have quickly evolved to the stable concentration at that temperature. The natural pre-ageing treatment significantly delayed the formation of GP zones with a peak number density at 1 h ageing at 180°C (Fig. 6a), and delayed the formation of β″ with no β″ precipitate formed after 10 min artificial ageing. After 1 h ageing at 180°C, the number density of β″ precipitates (1.15×10^{23} m^{-3}) observed from the T4 sample was much lower than the number density of 3.29×10^{23} m^{-3} from the as-quenched sample (Fig. 6).

The precipitate volume fraction has a strong correlation with the strengthening effect observed in the α-Al grains of the cast Al-7Si-0.6Mg alloy. This is evident by comparing the relative solute-concentration reduction of the matrix (Fig.10) with the alloy's hardness data (Fig.1), since the relative solute-concentration reduction of the matrix should be directly related to the volume fraction of precipitates formed in the alloy. During 10 min ageing at 180°C, the relative solute-concentration reduction of the matrix of T4 samples showed no clear decrease, suggesting that no significant change of precipitate volume fraction. This is consistent with little hardness change observed in Fig.1. The T4 sample aged for 1 h and the as-quenched sample aged for 10 min were observed with the same relative solute-concentration reduction of the matrix and

similar hardness as well. Similarly, the T4 sample and as-quenched sample aged for 4 h at 180°C were observed with a similar level of solute concentration reduction and again the same hardness was observed. Careful APT characterisations, as shown in Figs. 4-6, confirmed the coexistence of solute clusters, GP zones and β″in the primary grain of the alloy in the peak hardness condition. All those nanostructures are responsible for strengthening the alloy. Interestingly, the size, number density and composition of solute clusters, GP zones and β″ in the alloy were evolved differently with the increase in ageing time. Such complexity of solute nanostructures has not been fully considered in previous modelling of Al-Mg-Si-(Cu) wrought alloys [38]. It is expected that the prediction power of a theoretical model will be further enhanced by successfully incorporating the strengthening effect of all solute-nanostructures.

5. Conclusions

- The precipitation sequence in the primary α-Al of the casting Al-7Si-0.6Mg alloy F357 up to the peak aged condition (180^{o}C-4h) can be expressed as SSSS → solute clusters → solute clusters + GP-zones → solute clusters + GP-zones + β″. A natural pre-ageing for 120 h has no influence on the precipitation sequence of the alloy, but affects precipitation kinetics during initial 1 h ageing at 180°C.
- The natural pre-ageing slowed down the precipitation kinetics six- fold during the 1 h ageing, but such effect diminished after 4 h when the alloy reached the same hardness as that of an as-quenched sample.
- The number density of β″-needles formed in the primary α-Al grains of the naturally pre-aged sample is approximately half of that of the as-quenched sample. A 1-h ageing of the as-

quenched sample at 180°C promoted the formation of β″-needles at a high number density, as the alloy reached its peak hardness.

- The Mg:Si ratio of the early solute-clusters in the alloy in T4 condition is ~ 0.6, less than 0.7 observed in the alloy aged for 10 min at 180°C. The ratio of GP zones increases from 0.8 to 0.9 with increasing in their size, so does the Mg:Si ratio of β″ precipitates increases from 0.9 to 1.2. This indicates that the formation of the metastable phases involve enhanced partitioning of Mg.

- The precipitate volume fraction is an important parameter for strengthening the alloy. Solute clusters, GP-zones and β″ needles are responsible for the peak harness of the alloy. A hardness plateau between 1 h and 4 h ageing corresponds to the growth of β″ precipitates and concurrent decrease of solute clusters and GP zones.

Acknowledgments

The Department of Science and Technology (DST) in South Africa is acknowledged for funding under the Advanced Metals Initiative Program, as well as the technical, scientific and financial assistance from the AMMRF (Australian Microscopy and Microanalysis Research Facility). The contributions of U. Curle, D. Wilkins, A. Grobler, M. Williams and C. McDuling are also gratefully acknowledged.

References

1. Polmear I. Light alloys: from traditional alloys to nanocrystals. 4th ed. Oxford: Butterworth-Heinemann; 2006.
2. Rinderer B, Couper M, Xiong X, Gao S, Nie J-F. Mater Sci Forum 2010;654-656:590.
3. Banhart J, Chang CST, Liang Z, Wanderka N, Lay MDH, Hill AJ. Adv Eng Mater 2010;12:559
4. Vissers R, van Huis MA, Jansen J, Zandbergen HW, Marioara CD, Andersen SJ. Acta Mater 2007;55:3815
5. Zander J, Sandström, R. Mater & Des 2008;29:1540.
6. Buha J, Lumley RN, Crosky AG. Phil Mag 2008;88:373.
7. Vaumousse D, Cerezo A, Warren PJ. Ultramicroscopy 2003;95:215
8. Murayama M, Hono K. Acta Mater 1999;47:1537.
9. Edwards GA, Stiller K, Dunlop GL, Couper MJ. Acta Mater 1998;46:3893.
10. De Geuser F, Lefebvre W, Blavette D. Philos Mag Letter 2006;86:227.
11. Serizawa A, Hirosawa S, Sato T. Metal Mater Trans A 2008;39A:243.
12. Marioara CD, Andersen SJ, Jansen J, Zandbergen HW. Acta Mater 2003;51:789.
13. Chang CST, Wieler I, Wanderka N, Banhart J. Ultramicroscopy 2009;109:585.
14. Abid T, Boubertakh A, Hamada S. J Alloys Compd 2010;490:166.
15. Royset J, Stene T, Saeter JA, Reiso O. Mater Sci Forum 2006;519-521:239.
16. Yamada K, Sato T, Kamio A. Mater Sci Forum 2000;331–337:669.
17. Möller H, Govender G, Stumpf WE, Pistorius PC. Int J Cast Met Res 2010;23:37.
18. Möller H, Govender G, Stumpf WE. Int J Cast Met Res 2007;20:340.
19. Möller H, Govender G, Stumpf WE. Solid State Phenom 2008;141-143:737.

20. Sjölander E, Seifeddine S. J Mater Process Tech 2010;210:1249.
21. Bruwer R, Wilkins JD, Ivanchev LH, Rossouw P, Damm OFRA. US Patent No. 7368690 2008.
22. Miller MK. Atom probe tomography: analysis at the atomic level. New York: Kluwer Academic/Plenum Publishers; 2000.
23. Gault B, Moody MP, de Geuser F, Tsafnat G, La Fontaine A, Stephenson LT, et al. J Appl Phys 2009;105:034913.
24. Moody MP, Gault B, Stephenson LT, Haley D, Ringer SP. Ultramicroscopy 2009;109:815.
25. Marceau RKW, Sha G, Ferragut R, Dupasquier A, Ringer SP. Acta Mater 2010;58:4923.
26. Sha G, Cerezo A. Acta Mater 2004;52:4503.
27. Sha G, Marceau RKW, Gao X, Muddle BC, Ringer SP, Acta Mater 2011;59:1659.
28. Möller H, Govender G, Stumpf WE, Knutsen RD. Int J Cast Met Res 2009;22:417.
29. Yang W, Wang M, Zhang R, Zhang Q, Sheng X. Scripta Mater 2010;62:705.
30. Wanderka N, Lazarev N, Chang CST, Banhart J. Ultramicroscopy 2011; 111:701.
31. Matsuda K, Naoi T, Fujii K, Uetani Y, Sato T, Kamio A, Ikeno S. Mater Sci Eng A 1999;262:232.
32. Marioara CD, Andersen SJ, Jansen J, Zandbergen HW. Acta Mater 2001;49:321.
33. Taylor, JA, StJohn DH, Couper MJ. Aluminum Trans 2001;4-5:111.
34. Du Y, Chang YA, Huang B, Gong W, Jin Z, Xu H, et al. Mater Sci Eng A 2003;363:140.
35. Hasting HS, Froseth AG, Andersen SJ, Vissers R, Walmsley JC, Marioara CD, Danoix F, Lefebvre W, Holmestad R. J Appl Phys 2009;106: Article number 123527.
36. Gupta AK, Lloyd DJ, Court SA. Mater Sci Eng A 2001;316:11.
37. Sha G, Cerezo A. Acta Mater 2005;53:907.

38. Esmaeili S, Lloyd DJ. Acta Mater 2005;53:5257.

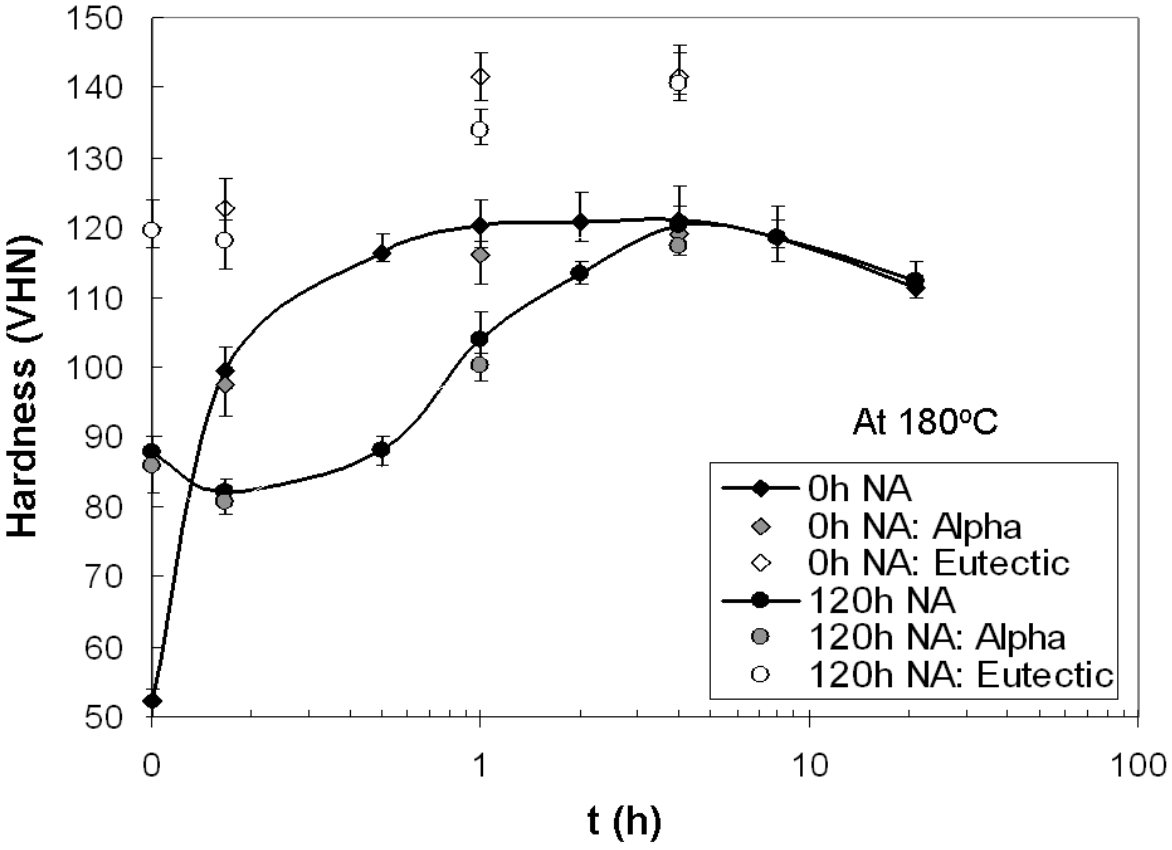

Figure 1: Artificial ageing curves for SSM-HPDC alloy F357 following no or 120 h of natural pre-ageing (NA), including the microhardness values of the primary α-Al and the eutectic components.

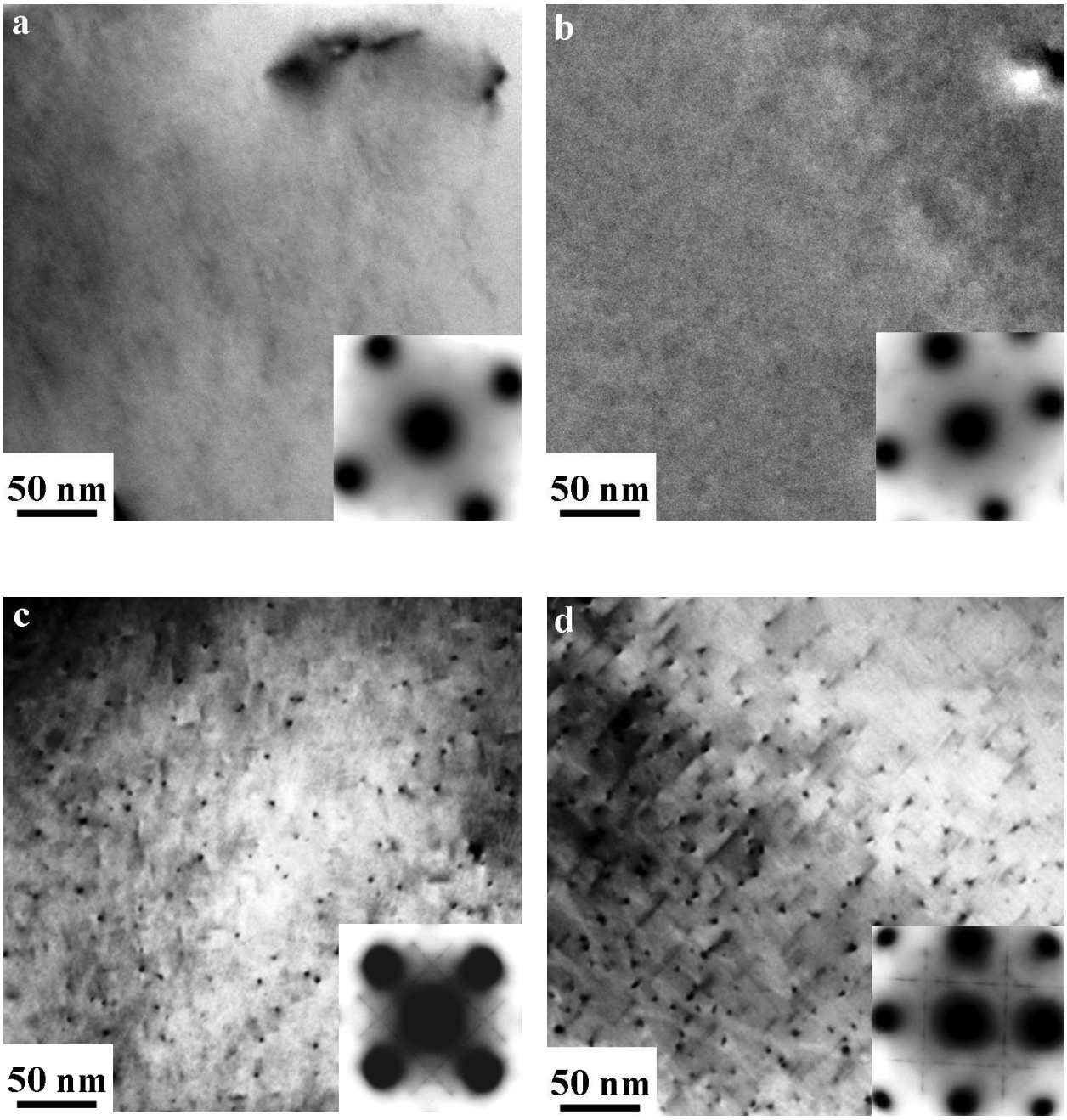

Figure 2: Bright field TEM images and SADPs for SSM-HPDC alloy F357 artificially aged at 180^{o}C for (a) 0 min, (b) 10 min, (c) 1 h and (d) 4 h after 120 h natural pre-ageing.

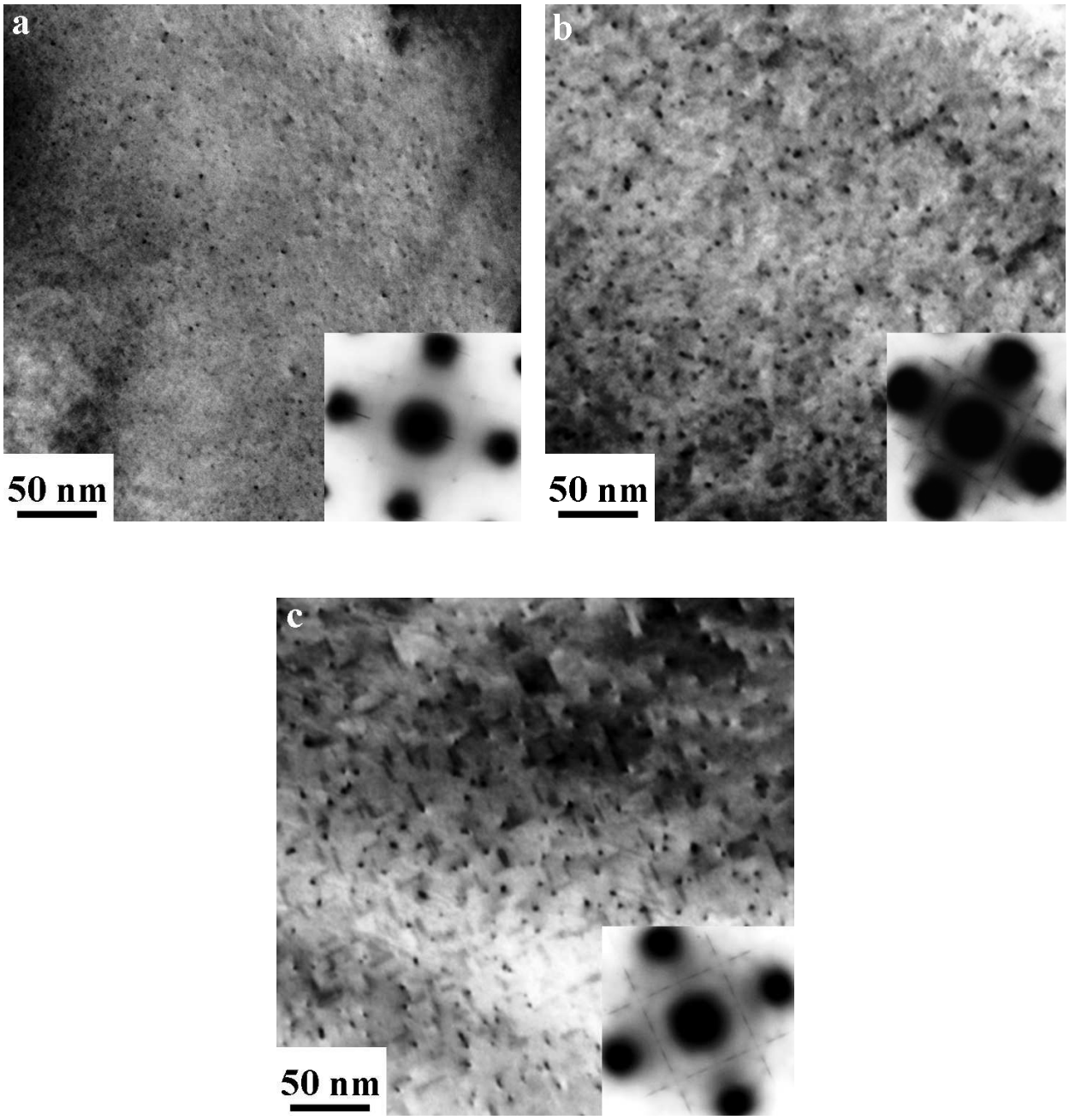

Figure 3: Bright field TEM images and SADPs for SSM-HPDC alloy F357 artificially aged at 180^{o}C for (a) 10 minutes, (b) 1 h and (c) 4 h after no natural pre-ageing.

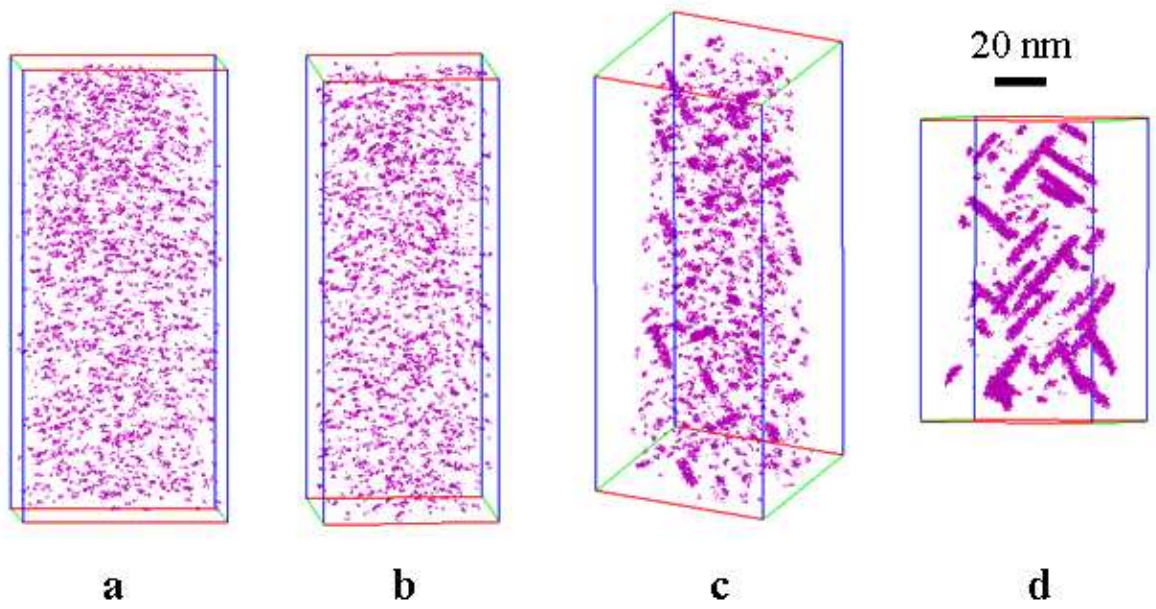

Figure 4: 3D Mg atom maps containing only solute enriched features after removing solutes in the matrix of SSM-HPDC alloy F357 aged at 180^{o}C for (a) 0 min, (b) 10 min (c) 1 h and (d) 4 h after 120 h prior natural ageing.

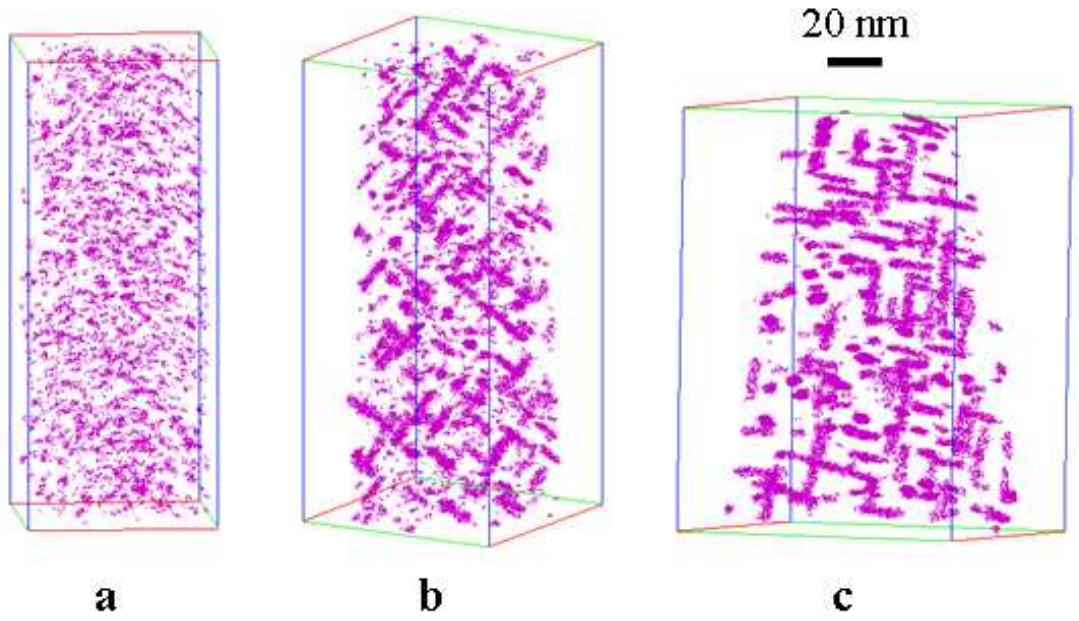

Figure 5: 3D reconstructed Mg atom maps containing only solute-enriched features after removing solutes in the matrix of SSM-HPDC alloy F357 artificially aged at 180^{o}C for (a) 10 min (b) 1 h and (c) 4 h after no prior natural ageing.

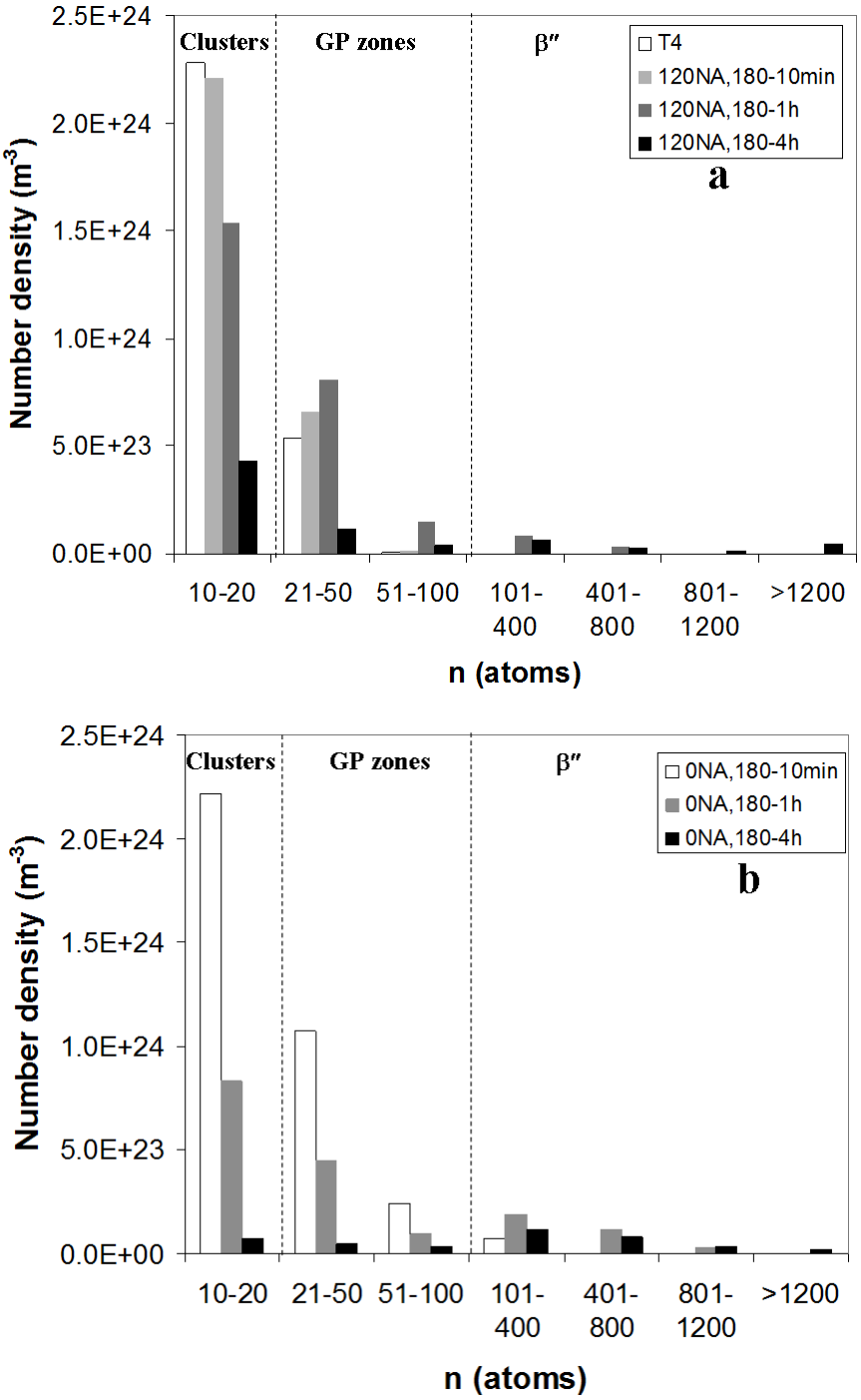

Figure 6: The evolution of the number density of precipitates in SSM-HPDC alloy F357 artificially aged at 180^{o}C following (a) 120 h natural pre-ageing, and (b) without the pre-ageing.

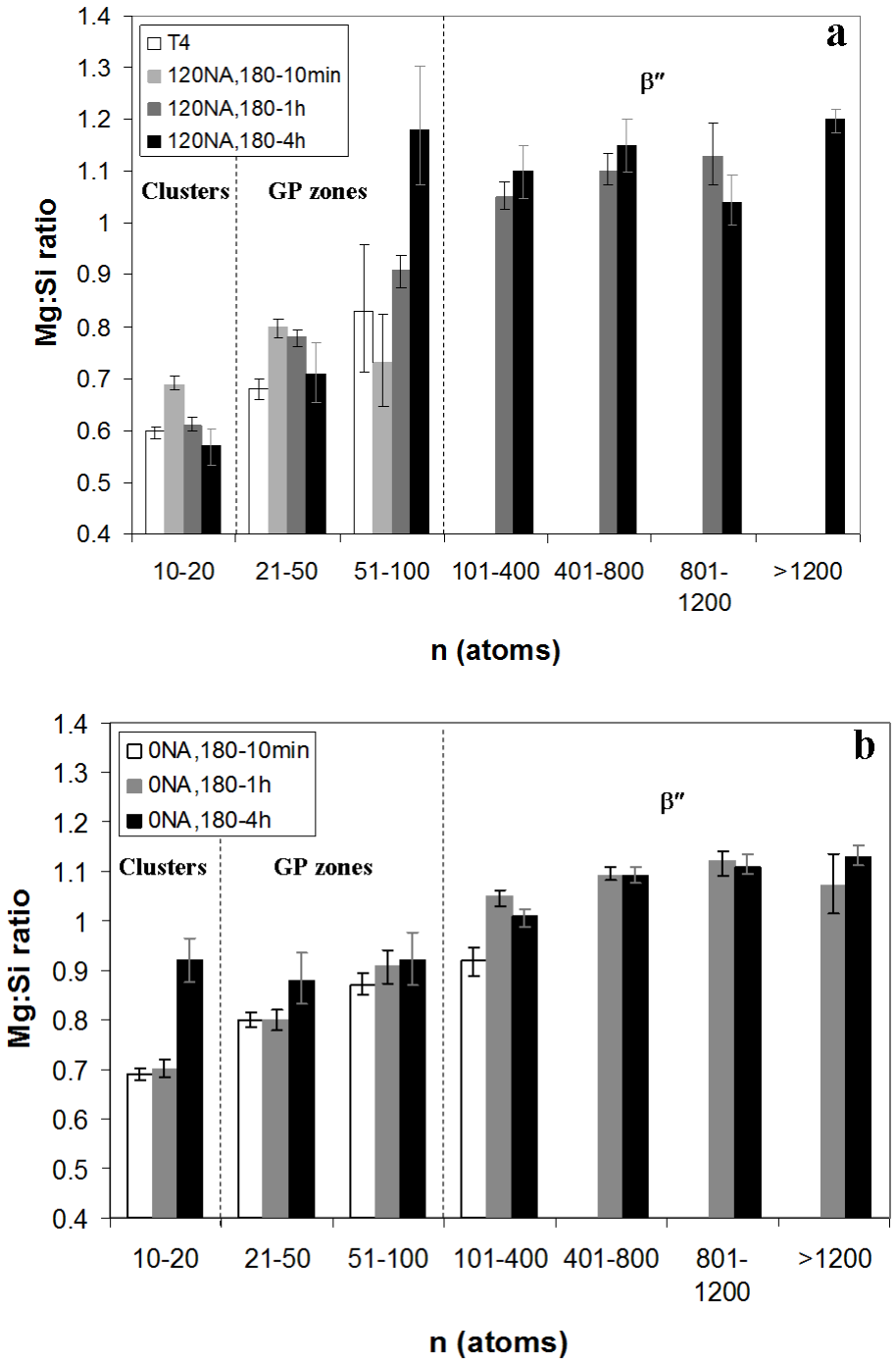

Figure 7: The evolution of Mg:Si ratio of solute clusters, GP zones and β″-needles in SSM-HPDC alloy F357 during ageing at 180^{o}C (a) with natural pre-ageing for 120 h, and (b) without the pre-aging treatment.

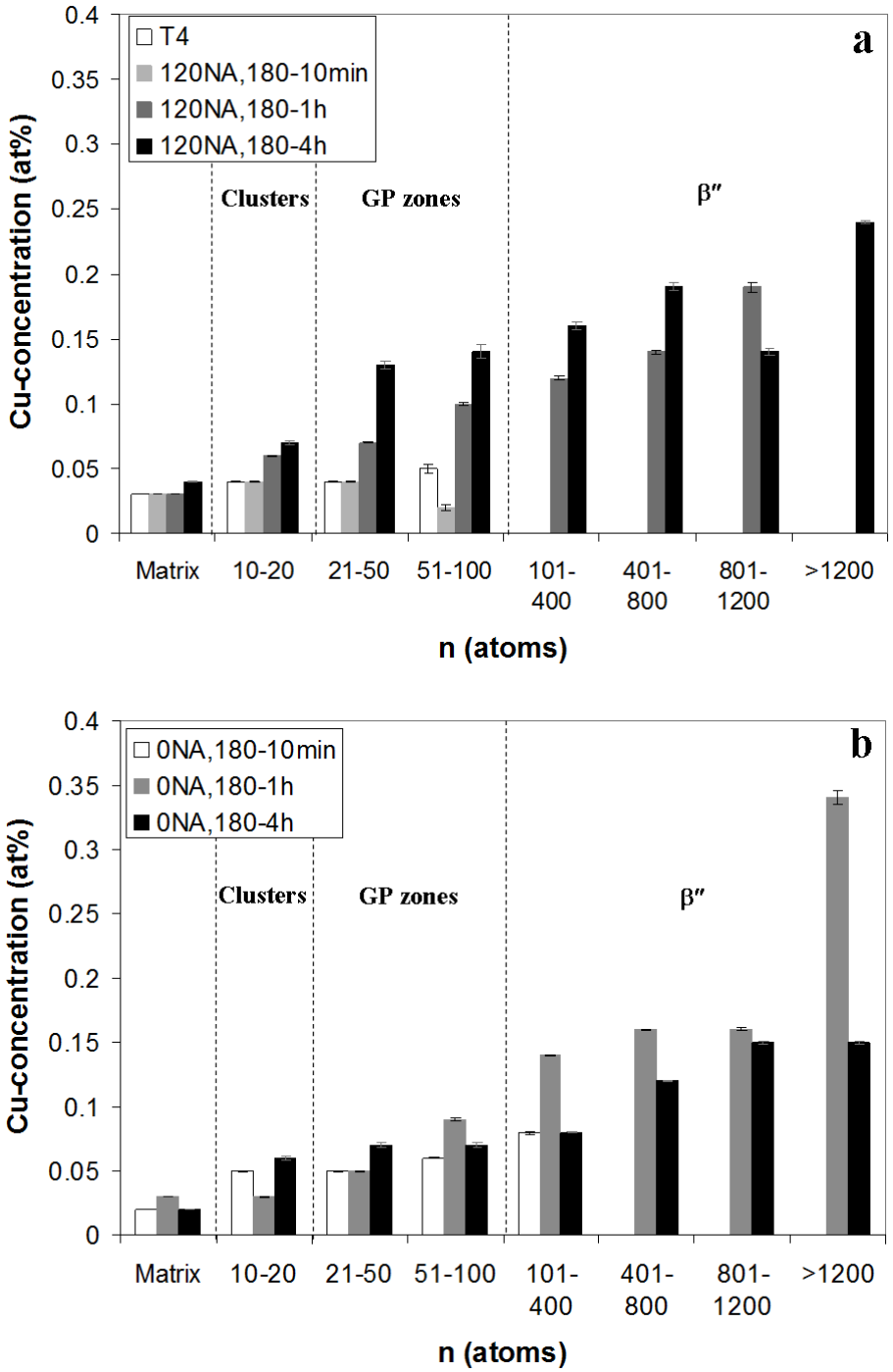

Figure 8: The evolution of the Cu content of the clusters/precipitates in SSM-HPDC alloy F357 artificially aged at 180^{o}C following (a) 120 h natural pre-ageing, and (b) without the pre-ageing.

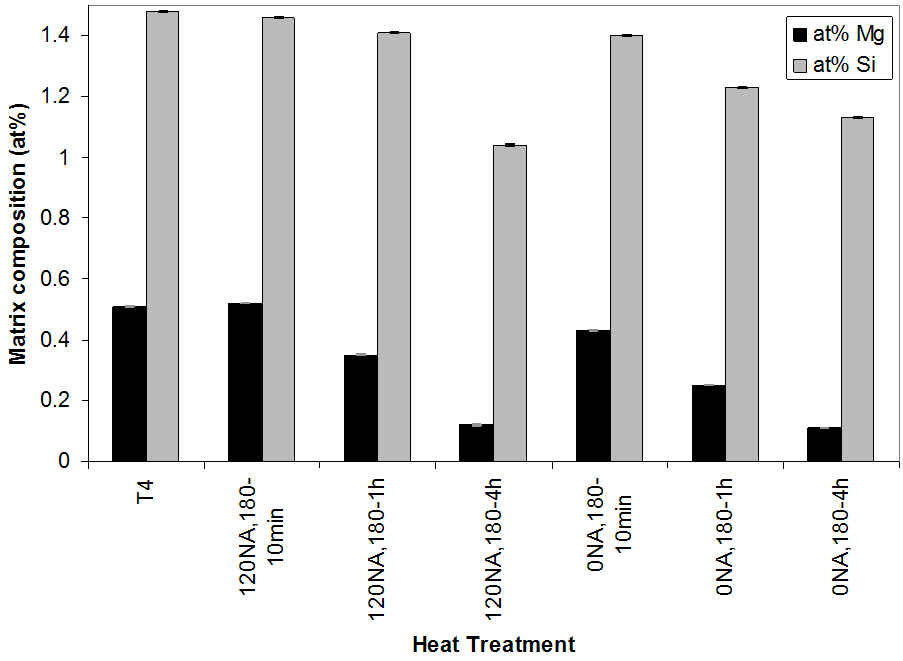

Figure 9: The Mg and Si concentration evolution of the matrix of SSM-HPDC alloy F357 with/without a natural pre-ageing treatment during artificial ageing at 180°C.

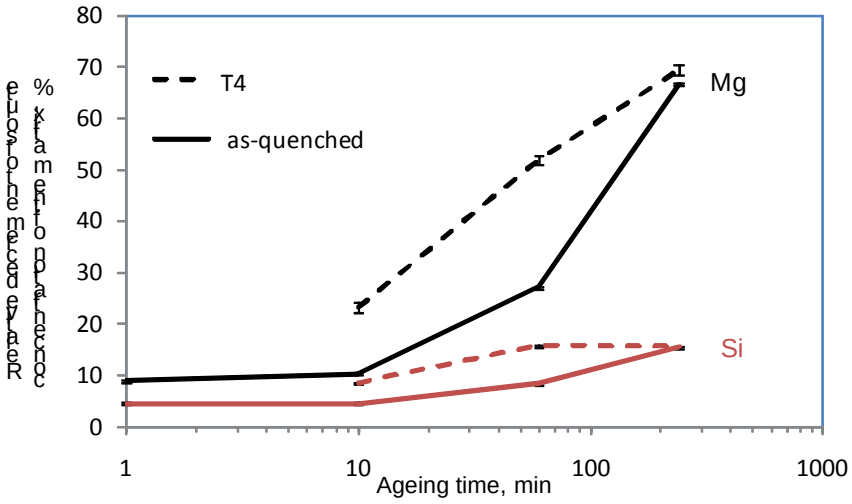

Figure 10: The relative decrements of solute concentration of the matrix measured in T4 samples and as-quenched samples of SSM-HPDC alloy F357 during ageing at 180°C.

Table 1: Chemical composition of SSM- high pressure die casting (HPDC) alloy F357.

	Si	Mg	Fe	Ti	Cu	Mn	Zn	Sr	Al
wt%	6.8	0.49	0.13	0.13	0.04	0.01	0.06	0.02	Balance
at%	6.6	0.54	0.06	0.07	0.02	0.005	0.02	0.006	Balance

Table 2: Tensile properties of SSM-HPDC alloy F357.

	YS (MPa)	**UTS (MPa)**	**% Elongation**
T4	176 ± 4	299 ± 2	18.0 ± 1.9
120 h NA,180^{o}C-10 min	164 ± 3	288 ± 3	20.2 ± 0.9
120 h NA,180^{o}C-1 h	253 ± 10	335 ± 4	11.7 ± 2.9
120 h NA,180^{o}C-4 h	303 ± 4	356 ± 4	10.6 ± 1.5
0 h NA,180^{o}C-10 min	180 ± 8	298 ± 3	19.1 ± 2.6
0 h NA,180^{o}C-1 h	288 ± 4	362 ± 2	12.5 ± 3.1
0 h NA,180^{o}C-4 h	304 ± 3	365 ± 3	10.6 ± 1.7